THE ASTROPHYSICAL JOURNAL, 483:402–413, 1997 July 1

MODULATIONAL INSTABILITY, MODE CONVERSION, AND RADIO EMISSION IN THE MAGNETIZED PAIR PLASMA OF PULSARS

JAMES C. WEATHERALL
Department of Physics, New Mexico Institute of Mining and Technology, Socorro, NM 87801
Received 1996 August 21; accepted 1997 January 27

ABSTRACT

A theoretical analysis of coupled mode equations describes the evolution of plasma wave turbulence in the strongly magnetized pair plasma of the pulsar polar cap. The onset of turbulence is a modulational instability of a large-amplitude electrostatic wave. Numerical solution follows the nonlinear evolution toward a strongly turbulent state characterized by the multidimensional collapse of wave packets. The turbulence generates electromagnetic modes that can escape the plasma. The modulational conversion process provides a fairly simple scenario for pulsar emission: an electrostatic plasma wave instability and the subsequent modulational mode coupling to escaping radiation.

Subject headings: instabilities — plasmas — pulsars: general — radiation mechanisms: nonthermal

1. INTRODUCTION

The uncertainty surrounding the process responsible for pulsar radio emission persists even though many features about pulsars are well accepted. It is widely believed that the radio emission source region is a magnetosphere of pair plasma above a neutron star polar cap (Sturrock 1971; Ruderman & Sutherland 1975; Arons & Scharlemann 1979). A coherent plasma mechanism operates to produce the emission (Arons 1983; Melrose 1992), tapping into the free energy of nonthermal particle streams produced in the electrodynamic environment of the rotating neutron star (Goldreich & Julian 1969; Kennel, Fujimara, & Pellat 1979).

The instabilities that can take place in the pulsar polar cap plasma include the plasma two-stream instability. This instability can initiate collective plasma effects through plasma wave turbulence. Plasma waves in the solar wind due to flare particle streams, and in shock-generated streams in planetary magnetospheres, are directly measured by spacecraft (Lin et al. 1981; Gurnett et al. 1981) and connected to coherent emission. Coherent emission near the plasma frequency is also generated in laboratory plasmas with intense electron beams (Kato, Benford, & Tzach 1983). Relative streaming of the pair components in the pulsar magnetosphere develop because of strong electric fields in the vicinity of the star (Cheng & Ruderman 1977a). Controversies concerning the relevance of streaming instability to pulsars relate to inefficiencies in converting to radiation (Asseo, Pellat, & Rosado 1980; Hinata 1976), and questions whether the instability occurs at all, given broad momentum distributions in the pair streams (Buschauer & Benford 1977). However, an analysis of the energetics of the pair streams seems to show instability even when the temperature of pair distributions is taken into account (Weatherall 1994). The fact remains that the instability generates plasma waves that do not escape as radiation; therefore, a secondary conversion process must be involved. An issue closely connected to the conversion process is how the instability saturates.

In the model by Asseo, Pelletier, & Sol (1990), the plasma wave turbulence saturates as one-dimensional solitary waves: conversion to radiation occurs through the transverse structure imposed by the finite geometry of the plasma source region. In order to develop into such structures, the turbulence must remain electrostatic and intrinsically one-dimensional. This description of turbulence is largely speculative and is based on calculations that appear to show solitary waves as stable and persistent entities. However, the picture of turbulence that emerges from the work reported here is strikingly different.

This paper presents a turbulence model based on wave-mode equations coupled through a cubic nonlinearity; this model provides a complete description of the evolution of plasma wave turbulence in the pulsar plasma. Numerical solution of the equations shows the development of turbulence that is intrinsically multidimensional. For this model, the turbulence is seeded from a large-amplitude electrostatic wave, such as might be generated by the two-stream instability. (The large-amplitude wave is designated the "pump wave.") The onset of the turbulence is a secondary wave-wave instability involving a four-wave interaction: two growing waves and two pump waves (see Fig. 1). The growing modes beat resonantly with the pump mode, $\boldsymbol{k}_0$, through coupling with a transverse perturbation, $\boldsymbol{k}$:

$$\omega(\boldsymbol{k}_0 + \boldsymbol{k}) - \omega(\boldsymbol{k}_0) - \omega(\boldsymbol{k}_0 - \boldsymbol{k}) + \omega(\boldsymbol{k}_0) = 0 \, .$$

The four-wave interaction is known as a modulational instability (Nishikawa & Liu 1976; Vladimirov et al. 1995). The nonlinear development of the instability shows spatial filamentation and "collapse" of the electrostatic wave. Because modulationally stimulated waves have an intrinsic electromagnetic character and are superluminal, they can propagate through the plasma and escape as radiation. The mode conversion also removes energy from the two-stream–driven pump wave and saturates the growth of the primary instability. Therefore, the modulational instability plays a direct role both in the energy balance of the turbulence, and in the radio emission.

The quantitative features of the radio emission in this model are almost entirely controlled by the in situ microphysics of the source plasma. The global environment of the neutron star magnetosphere and polar cap current flow is reduced to elements of wave energy sources and sinks, according to rates of two-stream instability and escape of radiation. While insulating the present work from the troublesome uncertainty inherent in pulsar theory, the model lacks some of the detail that may turn out to be

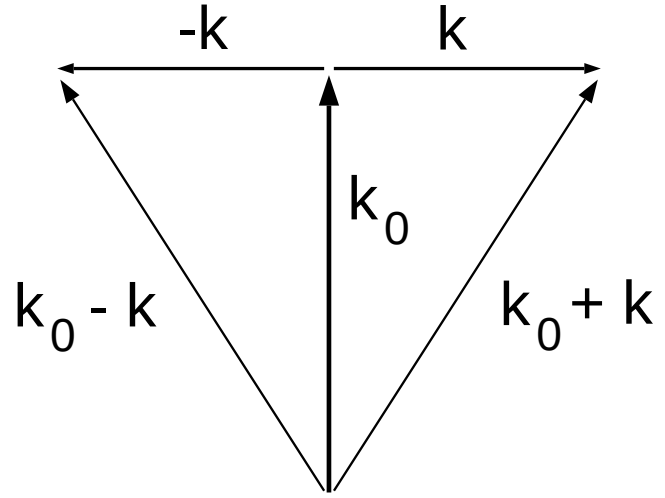

FIG. 1.—Momentum conservation for the modulational instability. $\boldsymbol{k}_0$ is the pump wavevector, $\boldsymbol{k}_0 \pm \boldsymbol{k}$ are the wavevectors of the modulational unstable modes, and $\boldsymbol{k}$ is the wavevector of the growing perpendicular perturbation.

necessary to fully describe the behavior of the pulsar emission. Most notable is the disregard of the kinematics of the plasma source by assuming that a frame exists in which the plasma is stationary and nonrelativistic. This assumption is discussed briefly in § 2.

In § 2, the theoretical model for the plasma wave turbulence is described. In § 3, a connection between the theoretical parameters defining the turbulence and the observed radio flux is provided. In § 4, analytical and numerical results for modulational instability are presented. The numerical coding for linear and nonlinear behavior is demonstrated on nonlinear wavepackets in the Appendix, and in § 4.1 by comparison with analytical instability formulas. In § 5 the wave turbulence evolution is followed through linear instability to wave collapse. The stability of one-dimensional solitons is explored in § 4.3. Differences in the underlying assumptions with the soliton model of Asseo et al. (1990) are made explicit in § 5. Finally, in § 6, the relevance of the modulational conversion process to pulsar emission is discussed.

2. NONLINEAR WAVE EQUATION

Maxwell's equations provide a complete description for the time evolution of the electromagnetic field:

$$\frac{\partial^2 \boldsymbol{E}(\boldsymbol{x}, t)}{\partial t^2} + c^2 \nabla \times [\nabla \times \boldsymbol{E}(\boldsymbol{x}, t)] = -4\pi \frac{\partial}{\partial t} \boldsymbol{j}(\boldsymbol{x}, t) . \quad (1)$$

When describing wavelike behavior at frequency ω, the plasma current is expressed in terms of a mobility tensor as a linear function of the electric field: $j_i = \sum (1/i4\pi\omega) M_{ij(s)} E_j$. The sum is over all plasma species, s—in this case the $s =$ " $-$ " denotes the electron, and $s =$ " $+$ " denotes the positron component. Plasma mobilities are derived through perturbation methods on plasma kinetic or fluid equations. Some interesting cases for magnetized pair plasmas are worked out by Arons & Barnard (1986). In the present case of stationary pairs in the large magnetic field limit, the currents are limited to the direction of the magnetic field. The nonzero component of the mobility tensor is given by

$$M_{\parallel(s)} = \hat{\boldsymbol{e}}_\parallel \cdot \boldsymbol{M}_{(s)} \cdot \hat{\boldsymbol{e}}_\parallel = \omega^2 \omega_{p(s)}^2 \int_{-\infty}^{+\infty} \frac{dv_\parallel f_{(s)}(v_\parallel)}{(\omega - k_\parallel v_\parallel)^2} . \quad (2)$$

The $\hat{\boldsymbol{e}}_\parallel$ axis aligns parallel to the magnetic field, and $f_{(s)}(v_\parallel)$ is the distribution function of velocities along the magnetic field direction. The description of wave behavior near the plasma frequency requires a high frequency limit of the mobility function:

$$\lim_{\omega \gg k_\parallel \bar{v}_{\parallel(s)}} M_{\parallel(s)} = \omega_{p(s)}^2 \left(1 + 3 \frac{k_\parallel^2 \bar{v}_{\parallel(s)}^2}{\omega^2}\right), \quad (3)$$

where $\bar{v}_{\parallel(s)}$ is the average of $v_\parallel$ over the distribution function. The component plasma frequency is defined by: $\omega_{p(s)}^2 = 4\pi n_{(s)} e_{(s)}^2 / m_{(s)}$. A low-frequency limit is also required to evaluate nonlinear currents from time averaged forces:

$$\lim_{\omega \ll k_\parallel \bar{v}_{\parallel(s)}} M_{\parallel(s)} = \omega^2 \left(-\frac{\omega_{p(s)}^2}{k_\parallel^2 \bar{v}_{\parallel(s)}^2}\right). \quad (4)$$

This treatment is nonrelativistic; the simulation of fully developed turbulence described in § 5 assumes a velocity spread of $\bar{v}_\parallel / c = 0.11$. This value derives from straightforward application of the theory of pair formation (Cheng & Ruderman 1977b; Sturrock 1971). Consider, for example, plasma pairs created by the destruction of 1 GeV gamma rays interacting with the magnetic field. Opacity for pair creation occurs at the location where the parameter $\chi = \frac{1}{2}(B \sin\psi)(\hbar e / m_e^2 c^3)(h\nu / m_e c^2)$ acquires a value of 0.15 with the changing angle ψ between the photon wavevector and the magnetic field (Arons & Scharlemann 1979). In the star frame, the momentum of the pairs has a mean of $\gamma\beta = \frac{1}{2}$ GeV$/(mc^2) \sim 1000$, with an uncertainty $\Delta\gamma\beta = 0.36\chi^{1/2} h\nu / (mc^2) \sim 140$ (Daugherty & Harding 1983). In the plasma frame, the momentum spread transforms to $\Delta\gamma\beta = 0.14$. The first generation of pairs is nonrelativistic in this frame.

Nonetheless, allowing for secondary pair cascades and an asymptotic kinetic current flow in the polar cap plasma, there may, in fact, be no reference frame in which the plasma can be regarded as either nonrelativistic or stationary. Clearly, such a current flow in a residual electric field needs to exist for the onset of the two-stream instability (Cheng & Ruderman 1977a). However, the appropriate momentum distributions have not been worked out in detail (although see Arons 1983; Weatherall 1994), and no attempt is made to incorporate any of the kinetic evolution here. Relativistic effects could be included in the present model by modifying the wave dispersion relation. The important linear feature of the waves, their dispersion in velocity, is extant when the plasma is relativistic.

2.1. *Wavemodes*

The wavelike solution $\boldsymbol{E} = \boldsymbol{A} \exp(i\omega t - i\boldsymbol{k} \cdot \boldsymbol{x})$, substituted into the linearized field equation, gives a matrix equation:

$$\begin{pmatrix} k_\parallel k_\parallel c^2 & 0 & -k_\parallel k_\perp c^2 \\ 0 & k^2 c^2 & 0 \\ -k_\parallel k_\perp c^2 & 0 & k_\perp k_\perp c^2 + M_\parallel \end{pmatrix} \begin{pmatrix} A_\perp \\ A_T \\ A_\parallel \end{pmatrix} = \omega^2 \begin{pmatrix} A_\perp \\ A_T \\ A_\parallel \end{pmatrix} . \quad (5)$$

Note that $A_\perp$ and $A_\parallel$ are vector components perpendicular and parallel to the magnetic field in the plane containing both the wavevector $\boldsymbol{k}$ and the magnetic field; A_T is the

vector component in the orthogonal direction. The eigenvalues and eigenvectors of the wave operator are associated with the frequencies $\omega(\boldsymbol{k})$ and the polarization vectors $\hat{\epsilon}(\boldsymbol{k})$ of the wavemodes in the system. Solution of the eigenvalue equation results in three orthogonal wavemodes. One of these is a purely transverse wave that does not couple to the plasma. The other two modes are denoted as an ordinary and an extraordinary wave (Arons & Barnard 1986). The frequency associated with the ordinary mode is given by

$$\omega_O^2 = k_\parallel^2 c^2 + \frac{Y + D}{2}, \tag{6}$$

and the normalized polarization vector is

$$\hat{\epsilon}_O = \frac{1}{[X^2 + (Y + D)^2]^{1/2}} \begin{pmatrix} X \\ 0 \\ Y + D \end{pmatrix}. \tag{7}$$

The frequency ω_X and polarization vector $\hat{\epsilon}_X$ for the extraordinary mode is obtained by taking $D \to -D$. The quantities in the above equations are defined as follows:

$$\begin{aligned} X &= 2k_\parallel k_\perp c^2 \ ; \\ Y &= \omega_p^2 - k_\parallel^2 c^2 + k_\perp^2 c^2 + 3k_\parallel^2 \bar{v}_\parallel^2 \ ; \\ D &= \sqrt{X^2 + Y^2} \ . \end{aligned} \tag{8}$$

The plasma frequency is given by the sum of electron and positron terms, $\omega_p^2 = \omega_{p(+)}^2 + \omega_{p(-)}^2$; the velocity parameter is defined as $\bar{v}_\parallel^2 = \bar{v}_{\parallel(-)}^2 + \bar{v}_{\parallel(+)}^2$.

The mode featured prominently in this theory is the fast branch of the ordinary mode when the wavenumber is small ($k_\parallel \lesssim \omega_p/c$). Because the electric field polarization is predominantly along the magnetic field direction, this mode couples strongly to the plasma. There is no plasma damping of this branch of the ordinary mode because it is superluminous. The mode has characteristics of a longitudinal plasma oscillation for wavevectors in the direction of the magnetic field and of a transverse electromagnetic wave in the direction transverse to the field.

The frequency and polarization characteristics of the ordinary mode are exhibited as a wavenumber map in Figure 2.

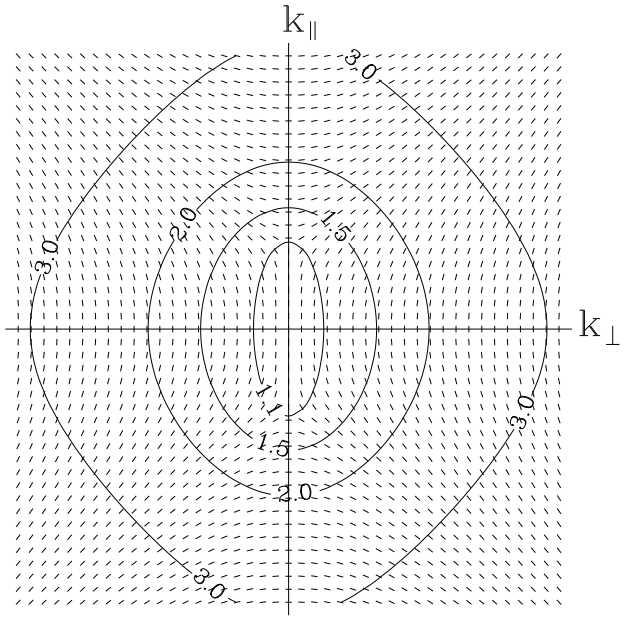

FIG. 2.—Contours of constant frequency of the ordinary mode in wavenumber space. Labels are in units of ω_p. The grid marks display the electric field polarization vectors. The wavenumber grid spacing is $0.16\omega_p/c$ in both the directions parallel and perpendicular to an infinite magnetic field. The plasma velocity dispersion is $\bar{v}_\parallel = 0.02c$.

2.2. *Wave Envelopes*

For treatment of waves for which ω is in the vicinity of the plasma frequency, it is useful to factor the fast-timescale oscillation and deal with an envelope function, $\hat{\boldsymbol{E}}(\boldsymbol{x}, t)$:

$$\boldsymbol{E}(\boldsymbol{x}, t) = \tfrac{1}{2}(\hat{\boldsymbol{E}} e^{i\omega_p t} + \hat{\boldsymbol{E}}^* e^{-i\omega_p t}) \ . \tag{9}$$

The equation that describes the slow-timescale modulation of the envelope function becomes

$$\begin{aligned} -2i\omega_p \frac{\partial}{\partial t} \hat{\boldsymbol{E}} = &+ c^2 \nabla \times (\nabla \times \hat{\boldsymbol{E}}) \\ &- 3\bar{v}_\parallel^2 \nabla_\parallel \nabla_\parallel \cdot \hat{\boldsymbol{E}} - \omega_p^2 (\boldsymbol{I} - \hat{\boldsymbol{e}}_\parallel \hat{\boldsymbol{e}}_\parallel) \cdot \hat{\boldsymbol{E}} \ . \end{aligned} \tag{10}$$

Note that a term $\partial^2 \hat{\boldsymbol{E}}/\partial t^2$ has been discarded. This is because modulations are assumed to be on a much slower timescale than the plasma oscillation period. Also, a term $\omega_p^2 \hat{\boldsymbol{E}}$ cancels with the linear current. This linear equation can be solved by a Fourier series expansion in the eigenmodes of the last section: a general solution as a linear superposition of wavemodes with amplitudes A_{mn} is

$$\hat{\boldsymbol{E}}(x, t) = \sum_{pol} \sum_{m=-\infty}^{+\infty} \sum_{n=-\infty}^{+\infty} A_{mn}(t) \hat{\epsilon}_{mn} e^{-ik_m x_\parallel - ik_n x_\perp} \ . \tag{11}$$

The solution of the linear wave equation is $A_{mn}(t) = A_{0mn} \exp[i(\omega_{mn} - \omega_p)t]$. In the finite volume L^2, the wavenumbers are $k_m = 2\pi m/L$ and $k_n = 2\pi n/L$. The frequency ω_{mn} denotes the frequency of the mode with wavevector $k_m \hat{\boldsymbol{e}}_\parallel + k_n \hat{\boldsymbol{e}}_\perp$. The finite series transform is convenient for numerical coding. One can generalize to a Fourier transform in the limit $L \to \infty$. The use of two dimensions, rather than three, is also for reasons of numerical efficiency. Plasma wave turbulence differs qualitatively from one– to many-dimensional solutions (Goldman & Nicholson 1978; Goldman 1984; Zakharov 1972), but the essential feature of the turbulence in space (Robinson, Newman, & Goldman 1988), namely, the "collapse," or self-focusing, of plasma waves, is adequately exhibited in two dimensions.

2.3. *Nonlinear Modulation*

Modification to the linear-wavemode solution is required to incorporate nonlinear effects on timescales that are distinct from the fast oscillation of the wave. The wavemodes are (weakly) coupled because of the beating of slow changes in plasma density with the linear plasma response to the wave, as shown in this section.

The slow-timescale evolution in the plasma can be described by a velocity drift $\delta v_{(s)} \hat{\boldsymbol{e}}_\parallel$ and density inhomogeneity $\delta n_{(s)}$ in the following manner:

$$\begin{aligned} \boldsymbol{v}_{(s)} &= \tfrac{1}{2}(\hat{v}_{(s)} e^{i\omega_p t} + \hat{v}_{(s)}^* e^{-i\omega_p t}) \hat{\boldsymbol{e}}_\parallel + \delta v_{(s)} \hat{\boldsymbol{e}}_\parallel \ ; \\ n_{(s)} &= \tfrac{1}{2}(\hat{n}_{(s)} e^{i\omega_p t} + \hat{n}_{(s)}^* e^{-i\omega_p t}) + \delta n_{(s)} + n_0 \ . \end{aligned} \tag{12}$$

In this two-timescale formulation, the modulated current, $\boldsymbol{j}^{\rm NL} = \frac{1}{2}[\hat{j}^{\rm NL} \exp(i\omega_p t) + \hat{n}^{*\rm NL} \exp(-i\omega_p t)]\boldsymbol{e}_{\parallel}$, has the form

$$\hat{j}^{\rm NL} e^{i\omega_p t} = \sum_s q_{(s)}[\delta n_{(s)} \hat{v}_{(s)} + \hat{n}_{(s)} \delta v_{(s)}] e^{i\omega_p t} . \quad (13)$$

An implicit assumption in this two-timescale separation is that the slow drift and local plasma density can be discovered through a time average over the plasma oscillation period, as denoted by $\delta v_{(s)} = \langle v_{(s)} \rangle$ and $\delta n_{(s)} = \langle n_{(s)} \rangle - n_0$. This means that the wave (fast-timescale) envelope functions $\hat{v}_{(s)}$ and $\hat{n}_{(s)}$ must be nearly constant over a plasma oscillation period. This restricts the turbulent wave model to wavemodes with linear frequencies ω_{mn} near the plasma frequency:

$$|\omega_{mn} - \omega_p| \ll \omega_p . \quad (14)$$

It also requires that the velocity drift, $\delta v_{(s)}$, and local density, $n_0 + \delta n_{(s)}$, be nearly constant over the plasma oscillation period. The validity of the two-timescale separation can be explored by examining the nonlinear timescales, T, associated with the modulational growth time. The evolutionary timescale must be such that $\omega_p T \gg 1$. Using the inverse modulational growth rate, as given in equation (33), for T gives

$$\omega_p T = \omega_p/\gamma \sim [E^2/16\pi n_0 m \bar{v}_{\parallel}^2]^{-1} . \quad (15)$$

Therefore, the requirement that $\omega_p T \gg 1$ is a constraint on the turbulent amplitude. The characteristic length, L, involved in the slow-timescale processes is also relevant. Let this length be the inverse modulational instability wavenumber, as inferred from the frequency mismatch condition leading to equation (33). Using a Taylor-series expansion for frequency mismatch, $\frac{1}{2}(d^2\omega/dk_{\perp}^2)k_{\perp}^2 \sim \gamma$, the wavenumber and wavelength are solved to obtain

$$L = \frac{2\pi}{k_{\perp}} \sim \frac{c}{\omega_p} (\omega_p T)^{1/2} . \quad (16)$$

Equations for the slowly varying plasma quantities are derived by time averaging Maxwell's equations and the plasma fluid equations. Of particular interest are the fluid momentum equations:

$$\frac{\partial\, \delta v_{(s)}}{\partial t} + \left\langle v_{(s)} \frac{\partial}{\partial x_{\parallel}} v_{(s)} \right\rangle - \frac{q_{(s)}}{n_0 m_{(s)}} \langle E \rangle - \frac{3\bar{v}_{\parallel(s)}}{n_0} \frac{\partial}{\partial x_{\parallel}} \delta n_{(s)} = 0 . \quad (17)$$

In solving for the slowly varying modulated current, the following approximations are allowed:

1. Ignore particle inertia, $\partial\, \delta v_{(s)}/\partial t \to 0$, in the fluid momentum equations. The inertia term is small compared with the pressure term when $L/T \sim c(\omega_p T)^{-1/2} \ll \bar{v}_{\parallel}$. This approximation is an adiabatic limit (Goldman 1984).

2. Assume no charge separation, $\langle E \rangle \to 0$, in the fluid momentum equations. This approximation of quasi neutrality applies when $L/T \ll \bar{v}_{\parallel}$. This also precludes a resonant low-frequency interaction (Hasegawa 1970).

3. Cross-field drifts are small in the large magnetic field limit because $v_{\perp}/(L/T) \sim 1/\omega_{\rm B} T \ll 1$, where $\omega_{\rm B}$ is the cyclotron frequency. In the large field limit, and with equal mass and magnitude of charge of the constituent plasma species, the slow-timescale motions are strictly one-dimensional.

4. The second-order density modulation is ignorable, $\langle \hat{n}_{(s)} \hat{v}_{(s)}^* + \hat{n}_{(s)}^* \hat{v}_{(s)} \rangle \to 0$ in the continuity equation. The fast-timescale motions time-average to zero because, in the wave oscillation, the fluid density and velocity changes are exactly out of phase.

5. The velocity modulation of the current is small, $\hat{n}_{(s)} \delta v_{(s)} \ll \delta n_{(s)} \hat{v}_{(s)}$. Comparing these terms when $\delta v_{(s)} \sim L/T$ and $\hat{v} \sim (\hat{n}_{(s)}/n_0)(\omega_p/k)$ shows the inequality holds when $(\omega_p T)^{-1/2} c \ll \omega_p/k \sim c$.

These approximations are appropriate when the parameter $(\omega_p T)^{-1}$ is small, the velocity dispersion in the plasma is large, and $\omega_{\rm B} \gg \omega_p$.

It follows that the nonlinear density modulation, $\delta n_{(s)}$, is due to a ponderomotive effect, as given by (Sanuki & Schmidt 1977):

$$\delta n_{(s)}(\boldsymbol{k}, \omega) = \frac{i n_{(s)}}{m\omega^2} \frac{k_{\parallel} M_{\parallel(s)}}{\omega_{p(s)}^2} \Psi_{\parallel(s)}(\boldsymbol{k}, \omega) , \quad (18)$$

where $\Psi_{\parallel(s)}(\boldsymbol{k}, \omega)$ is the Fourier transform of the ponderomotive force (Schmidt 1966; Gurevich & Pitaevskii 1963),

$$\Psi_{\parallel(s)}(x, t) = m_s \left\langle v_{(s)} \frac{\partial}{\partial x_{\parallel}} v_{\parallel(s)} \right\rangle = -\frac{1}{4} \frac{\partial}{\partial x_{\parallel}} \frac{q_{(s)}^2 \hat{E}_{\parallel}^* \hat{E}_{\parallel}}{\omega_p^2 m_{(s)}} . \quad (19)$$

The nonlinear current derives from the product of the nonlinear density modulation, $\delta n_{(s)}$, and the first-order wave velocity, $\hat{v}_{(s)} = q_{(s)} \hat{E}_{\parallel}/(i\omega_p m_{(s)})$. Incorporating the nonlinear current into the equation for the electric field amplitude gives

$$+2i\omega_p \frac{\partial}{\partial t} \hat{\boldsymbol{E}} + c^2 \nabla \times (\nabla \times \hat{\boldsymbol{E}}) - 3\bar{v}_{\parallel}^2 \nabla_{\parallel} \nabla_{\parallel} \cdot \hat{\boldsymbol{E}} - \omega_p^2 (I - \hat{\boldsymbol{e}}_{\parallel} \hat{\boldsymbol{e}}_{\parallel}) \cdot \hat{\boldsymbol{E}} = \frac{1}{8\pi} \frac{\hat{E}_{\parallel} \hat{E}_{\parallel}^* - (\hat{E}_{\parallel} \hat{E}_{\parallel}^*)_{\rm ave}}{n_0 m \bar{v}_{\parallel}^2} \omega_p^2 \hat{\boldsymbol{e}}_{\parallel} \hat{\boldsymbol{e}}_{\parallel} \cdot \hat{\boldsymbol{E}} . \quad (20)$$

When all vector quantities are parallel to the direction of the background magnetic field, this equation reduces to the form of a nonlinear Schrödinger equation. This generalization has also been treated by Pelletier, Sol, & Asseo (1988) and Asseo et al. (1990).

Note that the essential assumptions in the two-timescale model are: wave frequencies ω_{mn} near ω_p and separable timescales, $\partial \hat{\boldsymbol{E}}/\partial t \ll \omega_p \hat{\boldsymbol{E}}$. Further simplification of the low-frequency interaction requires an adiabatic approximation, quasi neutrality, and a large magnetic field.

The two-timescale separation becomes suspect if the wave amplitudes vary significantly over a plasma period. During the simulations described in § 5, the timescales are clearly distinct even though the parameter in equation (15) becomes of order unity in the strongest turbulent excitation. The effects of large turbulent excitation are partly mitigated by integrating equation (18) to get

$$n_{(s)}(x, t) = n_0 \exp(-\Phi_{(s)}/k_{\rm B} T) , \quad (21)$$

where $\Phi_{(s)}$ is the ponderomotive potential (see eq. [19]). This form for the nonlinear density is used for the numerical simulations, and reduces to equation (20) to first order in $E^2/(8\pi n_0 k_{\rm B} T)$.

2.4. *Coupled Mode Equations*

Solution of the modified nonlinear Schrödinger equation is sought through the time-dependent evolution of the wave amplitudes, A_{mn}. Substituting the modal expansion into the

nonlinear equation,

$$\left(2i\omega_p \frac{\partial}{\partial t} + \omega_{mn}^2 - \omega_p^2\right) A_{mn} = c_{mn} \Lambda_{mn}^{(\mathrm{NL})} . \quad (22)$$

The modulation term on the right-hand side of the modified wave equation is the nonlinear term expanded on the same basis set as the wavemodes. The nonlinear term is the Fourier series component

$$\Lambda_{mn}^{(\mathrm{NL})} = \frac{1}{L^2} \iint \left[\frac{1}{8\pi} \frac{E_\parallel E_\parallel^* - (\hat{E}_\parallel \hat{E}_\parallel^*)_{\mathrm{ave}}}{n_0 m \bar{v}_\parallel^2} \right] \times \omega_p^2 \hat{E}_\parallel e^{ik_m x_\parallel + ik_n x_\perp} dx_\parallel dx_\perp . \quad (23)$$

The term in brackets is the nonlinear Schrödinger potential, normalized to the plasma kinetic energy. The coefficient c_{mn} derives from coupling geometry: writing the vector $\hat{e}_\parallel$ in the orthonormal basis of the polarization axes, $\hat{e}_\parallel = c_{mn} \hat{\epsilon}_O + d_{mn} \hat{\epsilon}_X$, gives

$$c_{mn} = \frac{1}{2} \left[\frac{X^2 + (Y + D)^2}{D^2} \right]^{1/2} \mathrm{Sgn}\,(Y + D) . \quad (24)$$

The extraordinary mode coupling term d_{mn} is given by replacing D with $-D$.

This equation is useful for computer solution, in which the Fourier transform is performed numerically. It is also used for an analytic perturbation analysis of a large-amplitude excitation of a single wavemode in § 4.1.

2.5. *Computer Solution of Modal Equation*

The computer solution uses a split-step Fourier algorithm (Nicholson & Goldman 1978) to advance the coupled equations for the amplitudes of 64 × 64 modes. The time advance is accomplished in two parts, which give the algorithm its name. In the linear step, the nonlinear term is discarded, and solution in time of the first-order differential equations can be exact. The nonlinear step discards the linear terms, and adjusts the wave amplitude according to the nonlinear term by a simple Eulerian method. The nonlinear term is evaluated from the total electric field amplitude. The wave electric field is constructed on a periodic spatial grid from the wave amplitudes and phases through a coherent wave addition (inverse Fourier transformation).

The method has proven successful in solutions of plasma wave turbulence based on Zakharov and Schrödinger equations (Nicholson & Goldman 1978; Weatherall, Nicholson, & Goldman 1983; Robinson et al. 1988). This application to vector fields is new. The correctness of the code is verified by comparison to analytical formulas for linear and nonlinear wave behavior (refer to § 4 and the Appendix). In its present form, the code is second-order accurate in time step Δt, as determined by the accuracy of energy conservation. The evaluation of the energy in the modes includes the magnetic energy.

3. WAVE NONLINEARITY IN THE PULSAR MAGNETOSPHERE

A measure of the wave nonlinearity in equation (22) is the ratio of the local electric field energy density, $u' = \hat{E}_\parallel'^2/(8\pi)$, to the plasma kinetic energy density, $n_0' m \bar{v}_\parallel'^2$. (In this section, primed quantities refer explicitly to measurements in the rest frame of the plasma; unprimed quantities are in the neutron star or laboratory frame.) The electromagnetic energy density in the radio emitting region of pulsars can be related to the radio flux. This makes an important connection between theory and observations.

The giant pulses observed from the Crab pulsar provide a concrete example. They have been observed with flux, F_ν, as high as 10^2–10^4 Jy on timescales of order $T = 60$ ns (Hankins 1971). The pulses are observed throughout the radio frequencies of 300–8000 MHz. However, they are narrowband phenomenon because there is little correlation in their intensities in different frequency bands (Heiles & Rankin 1971).

Consider a localized source region of radius R' emitting optically thin isotropic radiation with uniform power per unit volume P' in the rest frame of the plasma. The frequency is equal to the local plasma frequency ν_p'. The emissivity is

$$j_\nu' = \frac{P'}{4\pi} \delta(\nu' - \nu_p') . \quad (25)$$

In the center of the cloud, $I_\nu' = j_\nu' R'$. The mean energy density is computed to be $u_0' = R'P'/c$.

In the laboratory frame, the cloud has a velocity β toward the observer. Every plasma element has an emissivity j_ν. The flux emitted from the source is found by integrating $j_\nu \, dl \, \Omega \, d\Omega$ over the source. The flux *emitted* from the source in the lab frame is thusly

$$F_\nu = 4\pi j_\nu R_\parallel \frac{1}{3} \frac{(R_\perp)^2}{D^2} , \quad (26)$$

where $2R_\perp/D$ is the angle subtended by source at distance D. Note that the source is Lorentz contracted in the direction of the boost, $R_\parallel = R'/\gamma$, while $R_\perp = R'$. The apparent transverse size of the source is denoted by R, so that $R = R'$. The quantities in the plasma rest frame are derived from the emissivity transformation, $j_\nu = j_\nu' \nu'^2/\nu^2$, and the frequency transformation, $\nu = \nu'\gamma(1 + \beta)$. Also, the *received* flux gains an extra factor of $(1 + \beta)\gamma$ because of time compression of the received flux from the motion of the source. The observed frequency spectrum is a delta function at $\nu = \nu_p' \gamma(1 + \beta)$, and the frequency integrated flux *received* is

$$F = \gamma^3 (1 + \beta) \frac{8}{3} \frac{R^2}{D^2} u_0' c . \quad (27)$$

The bandwidth and size of the emission region must be estimated in order to compare the calculated flux with observations. If the narrowband emission is received in a pulse of length ΔT, the limiting bandwidth may be characterized as the inverse of this time, so that $F_\nu = F\pi\Delta T$. Assuming 60 ns for the extent of the pulse, the bandwidth is at least 5 MHz. (The bandwidth is greater if there is unresolved time structure.)

The size of the emission region is not well constrained by characteristic light travel time. This characteristic length, taking into account the relativistic effects due to motion of the source, is limited only to $R' < c\,\Delta T \gamma^2 (1 + \beta) \sim 3600\gamma^2$ cm. Since γ is several hundred, this size can be greater than the size of the polar cap, $(R_*^3 \Omega/c)^{1/2} = 8 \times 10^4 [0.033 s/P]$ cm. Inasmuch as the emission occurs above and within the polar cap region, the size of the source region must not be larger than $R = 10^5$ cm.

Based on these estimates for physical parameters, observed frequency $\nu = 2\gamma\nu_p'$, and distance $D = 6 \times 10^{21}$ cm, the computed radiative energy density in the Crab

source region is

$$\frac{u'_0}{n'_0 m\bar{v}'^2_{\|}} = 0.3\left[\frac{300}{\gamma}\right]\left[\frac{10^5\ \mathrm{cm}}{R}\right]^2\left[\frac{5\ \mathrm{GHz}}{\nu}\right]^2 \times \left[\frac{\Delta\nu}{5\ \mathrm{MHz}}\right]\left[\frac{500\ \mathrm{keV}}{m\bar{v}'^2_{\|}}\right]\left[\frac{F_\nu}{10^2\ \mathrm{Jy}}\right]. \quad (28)$$

Therefore, dimensionless energy densities less than or of order unity may be expected to produce radiation of intensity sufficient to power pulsars. Later, in § 5, the radiative energy density is found to be comparable to the saturated electrostatic pump wave energy density. To complete the picture, it is shown in the following section that dimensionless energy densities of order unity lead to strong modulational coupling between the pump (two-stream–driven) wave and radiative modes.

4. MODULATIONAL INSTABILITY

4.1. *Linear Growth Rates*

The stability of a single large-amplitude wave, $\boldsymbol{E} = E_0\hat{\boldsymbol{\epsilon}}_{MN}\cos(-k_M x_{\|} - k_N x_{\perp} + \omega_{MN} t + \phi_{MN})$, can be studied analytically. Assuming only small-amplitude excitation of other modes, $A_{mn} \ll A_{MN}$, the leading order nonlinear interactions are quadratic in $A_{MN}(t) = (E_0/2)e^{i\phi_{MN}}e^{i(\omega_{MN}-\omega_p)t}$ and first-order in A_{mn}. The modal equations for A_{mn} become

$$\left(2i\omega_p\frac{\partial}{\partial t} + \omega_{mn}^2 - \omega_p^2\right)A_{mn} = \Omega_{mn}^2 A_{mn} + \Omega_{2M-m,2N-n}^2 e^{-2i\phi_0}A^*_{2M-m,2N-n}\,. \quad (29)$$

A nonlinear parameter with units of frequency incorporates the nonlinear potential and coupling factors:

$$\Omega_{mn}^2 = \frac{E_0^2}{8\pi n m\bar{v}_{\|}^2}\,\omega_p^2(\hat{\boldsymbol{\epsilon}}_{MN}\cdot\hat{\boldsymbol{e}}_{\|})^2(\hat{\boldsymbol{\epsilon}}_{mn}\cdot\hat{\boldsymbol{e}}_{\|})c_{mn}\,. \quad (30)$$

Also, to simplify notation, $\phi_0 = \phi_{MN} + (\omega_{MN} - \omega_p)t$. Allowing time variation $e^{i\omega t}$ results in pairs of coupled equations:

$$\begin{aligned}&[-\omega_p^2 + \omega_{M+m,N+n}^2 + 2(-\omega - \omega_{MN} + \omega_p)\omega_p - \Omega_{M+m,N+n}^2]A_{M+m,N+n}e^{i\phi_0} = \Omega_{M-m,N-n}^2 A^*_{M-m,N-n}e^{-i\phi_0};\\ &[-\omega_p^2 + \omega_{M-m,N-n}^2 + 2(\omega - \omega_{MN} + \omega_p)\omega_p - \Omega_{M-m,N-n}^2]A^*_{M-m,N-n}e^{-i\phi_0} = \Omega_{M+m,N+n}^2 A_{M+m,N+n}e^{i\phi_0}\,. \end{aligned} \quad (31)$$

A dispersion relation is obtained by solving for zero determinant of the matrix equation for the mode pairs:

$$[\omega_+^2 - 2(\omega + \omega_0 - \omega_+)\omega_p - \Omega_+^2] \times [\omega_-^2 - 2(-\omega + \omega_0 - \omega_-)\omega_p - \Omega_-^2] = \Omega_+^2\,\Omega_-^2\,. \quad (32)$$

The upshifted, downshifted, and pump wave frequency increments have been defined as $\omega_+ = \omega_{M+m,N+n} - \omega_p$, $\omega_- = \omega_{M-m,N-n} - \omega_p$, and $\omega_0 = \omega_{MN} - \omega_p$; and the upshifted and downshifted nonlinear frequencies as $\Omega_+ = \Omega_{M+m,N+n}$ and $\Omega_- = \Omega_{M-m,N-n}$.

Equation (32) can be solved for the frequency ω. An imaginary component to the frequency indicates instability. An example of a modulational instability of a large-amplitude electrostatic wave is shown by a growth-rate map in Figure 3. Maximum growth occurs for modes with a finite $k_\perp$.

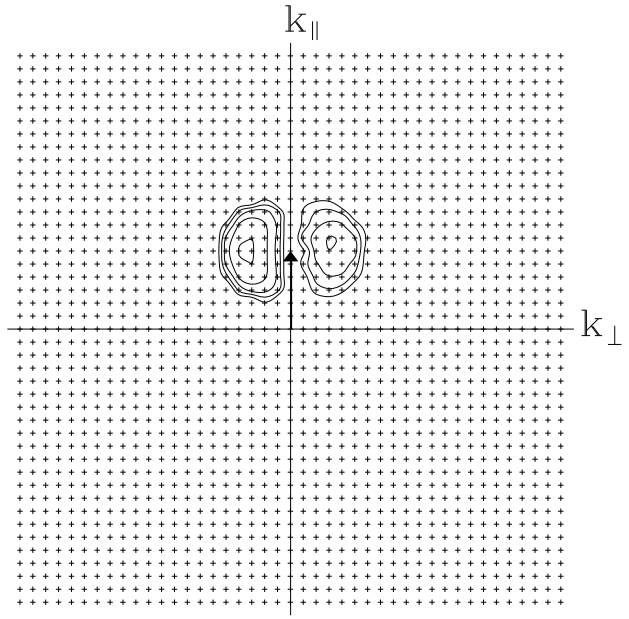

FIG. 3.—Contours of constant growth rate on the same wavenumber grid as in Fig. 2. The contours on the left are derived analytically, while those on the right are inferred from numerical solution. The arrow vector points to the pump mode with $k_0 = 0.95\omega_p/c$ and amplitude $E_0 = 0.867[8\pi n_0 m\bar{v}_{\|}^2]^{1/2}$. The velocity parameter is $\bar{v}_{\|}/c = 0.02$. Contour levels are 0.1, 0.15, 0.20, 0.25, and 0.30 ω_p.

The instability analysis indicates that the maximum growth rate occurs for modes with frequency mismatch $\omega_{M+m,N+n} - \omega_{MN} \sim \gamma$, where the maximum growth rate is

$$\frac{\gamma}{\omega_p} = \frac{\Omega^2}{2\omega_p^2} = \frac{1}{2}\,u_0\,. \quad (33)$$

Here, $u_0 = E_0^2/8\pi n_0 m\bar{v}_{\|}^2$ is the dimensionless energy density in the pump wave. This result follows from equation (32) by setting the geometric factors in the nonlinear coupling to unity and using $\Omega_+^2 \gg \omega_+^2$ and $\Omega_-^2 \gg \omega_-^2$.

4.2. *Nonlinear Development of the Modulational Instability: Wave Collapse*

Growth rates describe only the onset of turbulence in a plasma; it is also necessary to account for the subsequent behavior when the instabilities grow into substantial waves and couple not only to the pump mode, but to other modes. For this purpose, it is necessary to solve numerically for the phase and amplitude of a larger system of waves (here, 64×64 modes).

The numerical solution follows the evolution of the single large-amplitude mode of the previous instability analysis. The initial electric field of the wave is plotted in $(x_{\|}, x_\perp)$ space in Figure 4*a*.

A small amount of randomly phased noise is assigned to the other modes in the system. The instability of the wave is exhibited in Figure 4*b* as a transverse modulation. The fastest growing mode and growth rate correspond closely with the analytical instability theory. To show this, the growth rate of the instability can be derived from the numerical solution by computing for each mode $\gamma_{mn} = [\ln A_{mn}(t_2) - \ln A_{mn}(t_1)]/(t_2 - t_1)$, using times t_1 and t_2 early in the simulation. The resulting growth map is plotted along with the analytical growth rates in Figure 3.

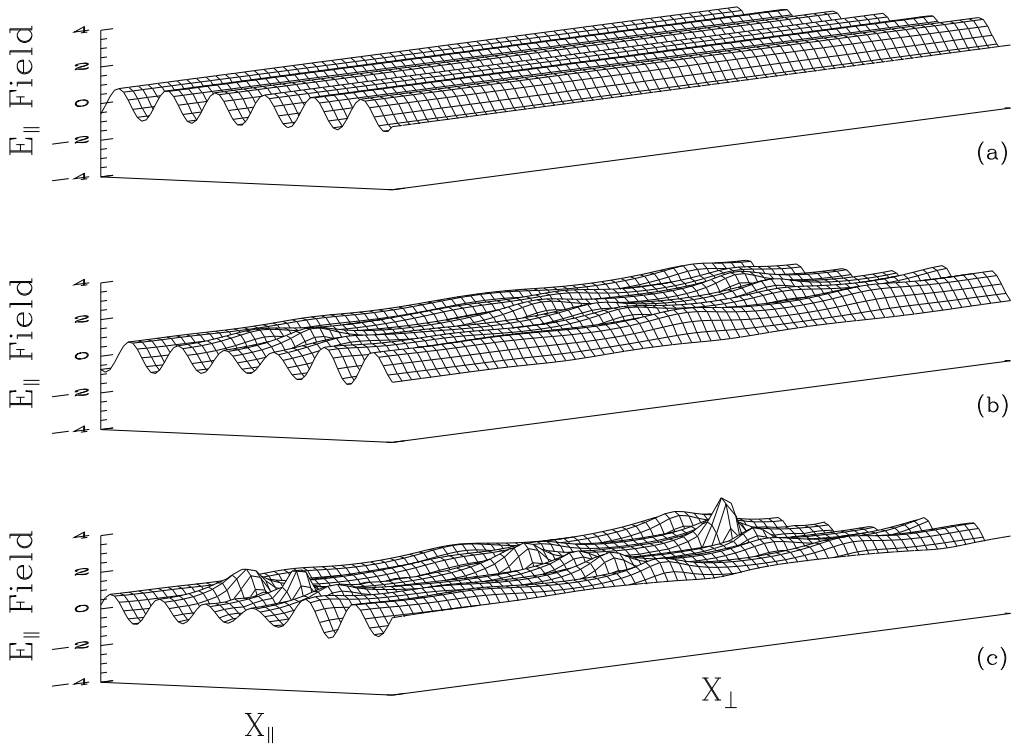

FIG. 4.—Surface plots of electric field on a two-dimensional 64 × 64 spatial grid that extends $40c/\omega_p$ along directions parallel and perpendicular to the magnetic field: (*a*) the initial large-amplitude pump wave of amplitude ± 0.867, scaled in units $[8\pi n_0 m\bar{v}_\parallel^2]^{1/2}$; (*b*) after 600 time steps ($30\omega_p^{-1}$), showing the onset of the modulational instability; (*c*) after 650 time steps ($32.5\omega_p^{-1}$), showing the increasing localization of the field at the modulated peaks.

Subsequent time evolution produces the wave structure in Figure 4*c*. Localized regions of high electric field develop out of the modulational instability. This is recognized as the phenomenon of plasma wave collapse, which is known to occur for unmagnetized electron-ion plasmas (Zakharov 1972; also see review by Goldman 1984).

It is interesting that the collapse occurs in the limit of *infinite* magnetic field. For the case of weakly magnetized electron-ion plasmas, the magnetic field is known to inhibit wave collapse (Newman, Goldman, & Ergun 1994; Pelletier et al. 1988; Zakharov 1975; Hadžievski et al. 1990; Goldman, Weatherall, & Nicholson 1981; Rowland 1985; Krasnosel'skikh & Sotnikov 1977). For this reason, a large background magnetic field is often assumed to make the system increasingly one-dimensional. The present case is somewhat different, however, because the ion species is the positron. But the essential difference is the fact that the present analysis includes coupling to *electromagnetic* wave-modes. The fact that these electromagnetic waves have transverse group velocities even for large magnetic field is vastly different from magnetized electrostatic turbulence.

4.3. *Instability of Solitons*

An exact, nonlinear solution to the Schrödinger-like wave equation is the soliton

$$\frac{\hat{E}_\parallel}{(8\pi n_0 m\bar{v}_\parallel^2)^{1/2}}\, e^{i\omega_p t} = A\ \mathrm{sech}\left[\frac{1}{L}(x - v_g t)\right] \exp\left[-ik_0(x - v_p t)\right], \quad (34)$$

where the soliton's width, phase velocity, and group velocity are:

$$\frac{L}{c\omega_p} = \sqrt{6}\,\frac{1}{A}\,\frac{\bar{v}_\parallel}{c};$$

$$\frac{v_p}{c} = \frac{\omega_p}{k_0 c}\left(1 + \frac{3}{2}\,\frac{k_0^2\bar{v}_\parallel^2}{\omega_p^2} - \frac{1}{4}\,A\right);$$

$$\frac{v_g}{c} = \frac{3k_0\bar{v}_\parallel}{\omega_p}\,\frac{\bar{v}_\parallel}{c}.$$

This is verified by substitution into the modified nonlinear Schrödinger equation (eq. [20]). One-dimensional solitons have been postulated as nonlinear wave excitations in pulsar plasmas (Asseo et al. 1990; Mikhailovskii, Onishchenko, & Tatarinov 1985; Mofiz et al. 1988). The behavior of solitary wave packets, which is an important demonstration of the correctness of the numerical solution, is described in the Appendix.

An important issue regarding the relevance of one-dimensional solitons to plasma turbulence is their stability. This is addressed through numerical solution of the nonlinear equation. The numerical code is initialized with a solitary wave with a wavenumber k_0 and amplitude A. The envelope of the initial solitary wave is shown in Figure 5. When transverse modes have zero amplitude, the wave propagates without dispersing. However, when the code is initialized with a small amplitude transverse perturbation, the subsequent evolution shows that the perturbation increases in an unstable fashion, as in Figure 5. Therefore, these solitary wave solutions are *not* stable, and suffer modulational instability to transverse perturbations.

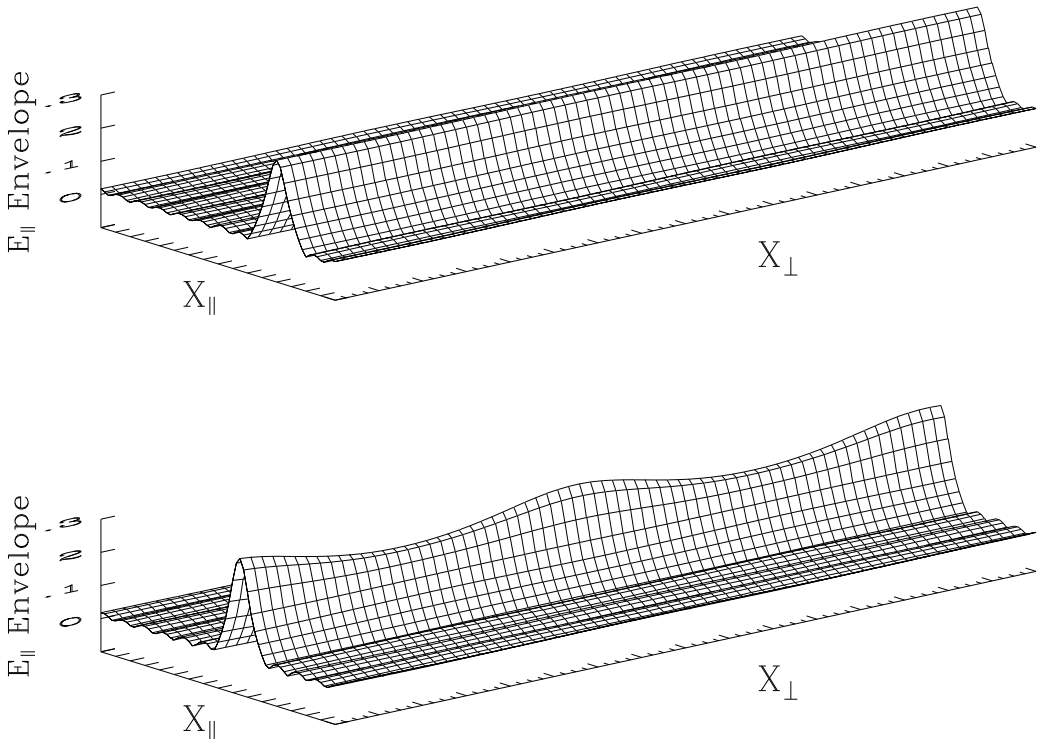

FIG. 5.—*Top*: Initial solitary wave; there is a small sinusoidal perturbation along $x_\perp$. *Bottom*: Soliton after 1500 timesteps ($150\omega_p^{-1}$), showing unstable growth of initial modulation.

This conclusion contradicts the result of Asseo et al. (1990), who establish the stability of the soliton-like solutions by applying an inverse-scattering transform perturbation method. The reason becomes apparent when one considers the linear dispersion relation for their wave-modes, which has the form $\omega^2 = \omega_p^2 + (k_\perp^2/k_\parallel^2)\omega_p^2$. This derives from the *slow* (Alfvén) branch of the ordinary mode of Arons & Barnard (1986), assuming both short wavelengths $k_\parallel \gg \omega_p/c$ and $k_\perp/k_\parallel \ll 1$. In contrast, the instability involves the fast branch in the wavelength region $k_\parallel \simeq \omega_p/c$.

Although the choice of the slow branch is appropriate for analyzing plasma modes that can be driven unstable by streaming instabilities, the emission model must include coupling to the fast-branch modes that propagate through and escape from the plasma (Arons & Barnard 1986). The use of a fast-branch mode as a pump wave in the simulations is not strictly correct, but can be justified because fast-branch modes with $k_\perp = 0$ and $k_\parallel \lesssim \omega_p/c$ have essentially identical dispersive and polarization characteristics to those of slow-branch modes with $k_\parallel \gtrsim \omega_p/c$, and the modes that are driven unstable by relativistic beams have wavenumbers $k_\parallel \sim \omega_p/c$.

5. FULLY DEVELOPED TURBULENCE: MODULATIONAL CONVERSION IN PULSARS

The full development of the turbulence in the pulsar plasma is followed through numerical solution of the coupled mode equations including energy sources and sinks.

The energy source, the relative streaming of the pair species, manifests itself in the wave system through the two-stream instability. The two-stream instability is modeled by incrementing the amplitude of a single pump mode in the system by the growth factor $\exp(\gamma_0 \Delta t)$, where Δt is the time step. The growth rate γ_0 is model-dependent. A characteristic growth rate $\gamma_0/\omega_p \sim 1.0 \times 10^{-3}$ is assumed (for example, Weatherall 1994). All numerical quantities in this section apply to the plasma frame, unless otherwise noted.

In the absence of damping of waves by particles, the energy loss to the wave system is by the escape of radiation. In the optically thin system of size R, the radiative loss occurs at a rate c/R. At the observed frequency of $\nu_{\rm obs} = 5$ GHz, a local plasma frequency of $\nu_p/\nu_{\rm obs} = (2\gamma)^{-1} \sim 10^{-3}$, and a source size $R = 2 \times 10^4$ cm, the basic loss rate is $\nu_{\rm loss}/\omega_p = c/(R\omega_p) = 0.05$. The energy loss to the system is implemented by decreasing each mode amplitude by a factor $|\hat{\boldsymbol{k}} \times \hat{\boldsymbol{\epsilon}}_O| \exp(-\nu_{\rm loss} \Delta t)$ during each time step. The loss formula includes a geometric factor that appears in the Poynting flux, $uc|\hat{\boldsymbol{k}} \times \hat{\boldsymbol{\epsilon}}_O|^2$. The energy time history of the turbulence is plotted in Figure 6. The evolution of the turbulence exhibits several stages:

1. The wave energy increases exponentially during the growth of a single monochromatic wave (pump wave) because of an external instability.
2. As the wave amplitude grows, it eventually stimulates the growth of modulational instabilities. Because these transverse modulations grow at the expense of wave energy in the pump wave, the modulational instability can saturate the pump wave growth.
3. The system reaches a fully developed turbulent state characterized by the rapid formation of intense localized wave packets (see Fig. 7). These collapsed wave structures are damped by the escape of radiation.
4. The system relaxes to a state of lower energy density. In this weakly turbulent state, when the instability growth time is long, one-dimensional soliton-like structures sometimes emerge.

Therefore, a slow buildup of energy in the system is followed by depletion in short bursts of radiation. Figure 6

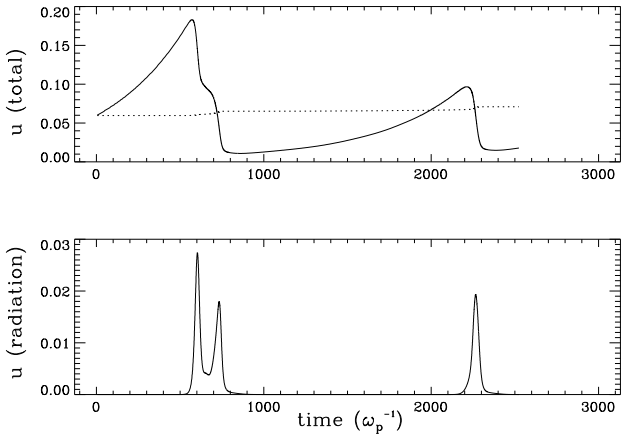

FIG. 6.—*Top*: Time history of total electric wave energy density in system, $u = E^2/(8\pi)$ normalized to kinetic energy density, $n_0 m\bar{v}_\parallel^2$. Dotted line indicates constancy of the total energy density of the system excluding energy added and removed by explicit growth and damping. *Bottom*: Time history of energy density in waves escaping the system by radiation, $u = \Delta(E^2 + B^2)/(8\pi v_{\rm loss}\,\Delta t)$. The bursts of radiation correspond to the saturation and depletion of wave energy in the top panel.

shows that the emission by modulational conversion is observed in the neutron star (lab) frame in bursts of 2–5 ns duration with amplitude of 3×10^{-3} Jy.[1] One can infer a brightness temperature of 10^{27} K.

6. DISCUSSION

The characteristics of the modulational mode-conversion mechanism have been specified by considering the microphysics of the nonlinear plasma behavior. The calculations are made as independently as possible of model-specific details relating to neutron star electrodynamics and the formation, location, and evolution of the polar cap plasma. The only external inputs to the computational solution of coupled mode equations are the plasma wave growth and mode damping. These are treated parametrically by growth and damping rates associated with two-stream instability and the escape of radiation. The value added by more detailed characterization of the plasma environment is weighed against the uncertainty introduced by additional parameters. The focus is on the essential physics of the plasma source, namely, the nonlinear wave dynamics.

The most important model-dependent feature that is being ignored is the kinetic evolution of the plasma, including bulk streaming and relativistic effects; these can modify the linear characteristics of the waves, the coupling, and the boundary conditions applied to the simulations. There are other simplifications in the model that should be noted. The geometry of the source region is treated very simply in its own rest frame with one length parameter: the source volume is Lorentz-contracted to a "pancake" in the neutron-star frame, a geometry that is somewhat arbitrary. The inference of the received flux from the in situ radiation energy density ignores details of the directivity and differential Doppler boosting of the emission. Simplifications implicit in the numerical algorithm include assumption of uniform plasma density, Cartesian geometry with two spatial degrees of freedom and periodic boundary conditions, and the inclusion of only ordinary wavemodes. The two-timescale separation in the coupled mode theory itself requires that the nonlinear evolution occurs on a timescale distinct from the linear mode oscillations, and is limited to modes with frequencies near the local plasma frequency.

Regardless of the uncertainties in the theory and the limitations in the numerical model, the nonlinear behavior that is essential to the emission phenomena is characteristic of the plasma itself and can be studied independently of the

[1] We invert eq. (28) to convert the in situ radiation energy density to received flux: $F_\nu = 10u(0.05\omega_p/\nu_{\rm loss})^2(\bar{v}_\parallel/c)^2$ Jy. The velocity parameter is $\bar{v}_\parallel/c = 0.11$. The plasma frequency in the plasma frame transforms to the radio wave frequency in the lab frame.

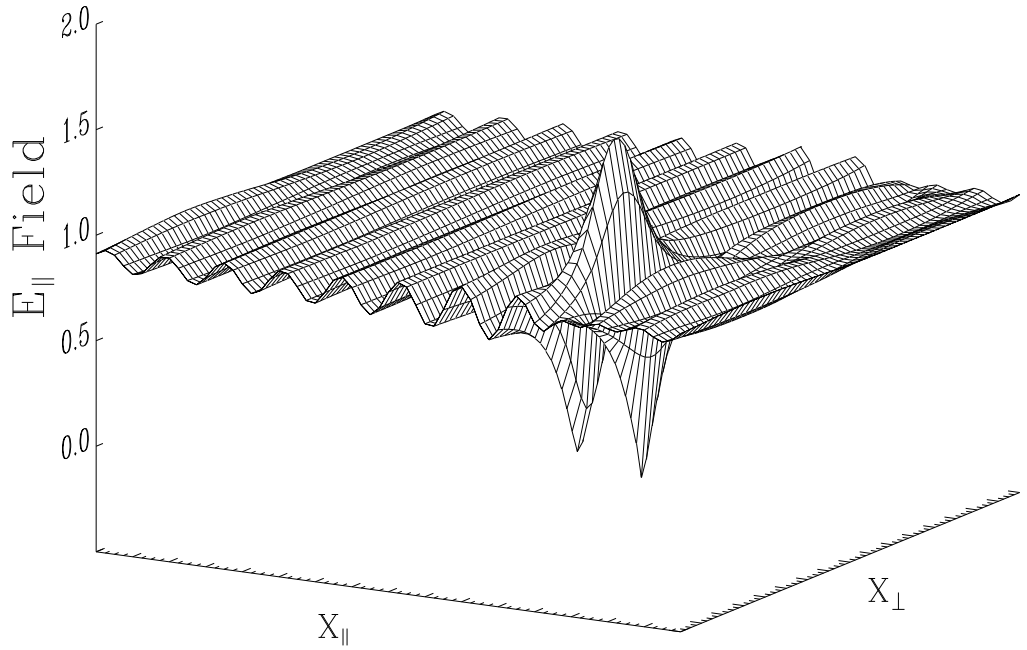

FIG. 7.—Surface plot of electric field envelope amplitude showing fully developed turbulence. Peak amplitude is $1.7(8\pi n_0 m\bar{v}_\parallel^2)^{1/2}$. Total grid size is $64\,c/\omega_p$ along $x_\parallel$ and $32\,c/\omega_p$ along $x_\perp$.

environmental features. One way to apply these results is to seek connections with observable features of the turbulence—for example, by matching the time evolution of the turbulence with the observed microstructure of the radio pulse. This will be attempted in future work.

The primary results of this analysis are based on computer solutions of coupled wave equations. The accuracy of the computational procedure is supported by comparison with both linear and nonlinear wave properties, namely, phase and group velocities of waves, instability wavelengths and growth rates, and soliton behavior. Energy conservation is verified during the transfer of wave energy between modes.

The modulational conversion process provides a fairly simple scenario for pulsar emission: an electrostatic plasma-wave instability and the subsequent modulational mode coupling to escaping radiation.

An important outcome of the numerical solutions is the fact that the turbulence is *not* one-dimensional. This is significant because amplitude variation transverse to the electrostatic wavevector is necessary to couple to the radiation field. This result for plasma turbulence can be compared with the nonlinear wave structures hypothesized by Asseo et al. (1990). They compute the conversion of essentially one-dimensional plasma turbulence to radiation by perturbation resulting from the finite transverse extent of the plasma. However, transverse perturbations can arise naturally through modulational instability: the turbulence develops a two-dimensional structure on smaller length scales than the Asseo model, which facilitates the radiative conversion. Although Asseo et al. (1990) dismiss such a role of transverse instability in the development of short wavelength turbulence, this is not true for the regime for which $k_{\|} c/\omega_p$ is of order unity.

In the broader context of plasma physics, the numerical solutions show that by including electromagnetic effects, plasma wave turbulence can "collapse" to smaller size, even in the limit of infinite magnetic field, when wavelengths are on the order of, or less than, the plasma skin depth, c/ω_p. This counters a prevalent view that magnetized electrostatic turbulence is intrinsically one-dimensional or limited to pancake-like wave packets.

Quantitative calculations show that the modulational conversion process is capable producing the intense coherent emission from pulsars. The numerical solutions show that the emission will occur in bursts. This underscores the possibility that nonlinear evolution of the wave turbulence can account for the fluctuations in the radio emission known as microstructure (Mofiz, de Angelis, & Forlani 1985; Asseo 1993; Chian 1992). Detailed numerical simulations offer an opportunity to formulate a definitive test of this theory against the observed microstructure. A full analysis of the temporal structure of the emission will be detailed in a separate paper.

This work is supported by NSF grant AST 93-15285. Discussions with Tim Hankins, Jean Eilek, Paul Arendt, and Dave Moffett are gratefully acknowledged. Thanks also to H. Beckley, who contributed to testing the numerical code and K. Marsh for help in editing the manuscript.

APPENDIX A

BEHAVIOR OF LINEAR AND NONLINEAR WAVEPACKETS

The behavior of linear and solitary plasma-wave packets is followed through numerical solution of the coupled mode equations. The results are compared with analytical formulas.

The numerical solutions apply to ordinary-mode waves (fast branch) in a pair plasma, in the infinite magnetic field limit. The mode propagates along the magnetic field, with $k_{\|} = k_0$ and $k_{\perp} = 0$. The frequency of such a wave, derived from the dispersion relation equation (6), is

$$\omega^2 \sim \omega_p^2 + 3k_0^2 \bar{v}_{\|}^2 , \tag{A1}$$

when $k_0 c/\omega_p \ll 1$. The phase and group velocities follow; $v_p = \omega/k_0$ and $v_g = d\omega/dk_0$. Also, a low-amplitude (linear) wavepacket of amplitude E and half-width at half maximum $L_{1/2}$ will spread after time t to $L_{1/2}(1 + \beta^2 t^2)^{1/2}$. The dispersion parameter is (Jackson 1975)

$$\beta^2 = \frac{1}{L_{1/2}} \frac{d^2\omega}{dk_0^2} . \tag{A2}$$

The initialization for the numerical runs are wavepackets with a hyperbolic-secant envelope:

$$\frac{\hat{E}}{(8\pi n_0 m \bar{v}_{\|}^2)^{1/2}} = A \text{ sech} \left[\frac{(x - x_0)}{L}\right] \exp\left[-ik_0(x - x_0)\right] . \tag{A3}$$

The numerical parameters are specified in Table 1. In the first example (run 1), the amplitude satisfies the analytical form of a solitary wave, $A = (6)^{1/2}(\bar{v}_{\|}/c)(c/\omega_p)L^{-1}$ (see eq. [34]). For this nonlinear wavepacket, the wave dispersion is offset by the nonlinear self-focusing. The numerical solution is shown in Figure 8.

Although the code solves for the fields on a two-dimensional spatial grid with 64 × 64 elements, only a one-dimensional cross section is displayed here (see, however, two-dimensional plots in Fig. 5). The grid spacing is $\Delta x_{\|} = 1.0 c/\omega_p$ and the time step is $\Delta t = 0.1\omega_p^{-1}$. Figure 8 displays the wave forms at three different times. Note that the soliton propagates without distortion.

The next example (run 2), shown in Figure 9, is the same wavepacket but with 10% of the energy of the solitary wave solution. As the wavepacket propagates, it spreads out, exhibiting the linear wave dispersion. The phase velocity (phase propagation distance divided by time) can be measured between Figures 9*a* and 9*b*, and the group velocity (envelope

TABLE 1

NUMERICAL PARAMETERS FOR WAVE PACKET SIMULATION

Symbol	Description	Value
k_0	Wavenumber	$0.59\omega_p/c$
L	Wavepacket width	$2.0c/\omega_p$
A	Amplitude	0.266 (run 1) 0.084 (run 2)
$\bar{v}_\parallel/c$	Plasma velocity parameter	0.2
v_{ph}	Phase velocity (theory)	$1.67c$
v_{gr}	Group velocity (theory)	$0.071c$
$L_{1/2}$	HWHM (actual)	$3.5c/\omega_p$
β	Dispersion parameter (theory)	$0.009\omega_p$

propagation distance divided by time) can be measured between Figure 9*a* and 9*c*. Note that the phase and group velocities of the solitary wave are comparable with the linear wave packet: nonlinear corrections occur only with larger amplitude. The rate of dispersion can also be measured. Table 2 summarizes wave parameters derived from the numerical runs and values computed from the analytical formulas. The numerical examples exhibit the correct linear and nonlinear behavior. Further corroboration of the numerical algorithm is found by comparing theoretical and numerical solutions for wave instability in §§ 4.1 and 4.2. The accuracy of the simulations is also tested through the conservation of energy.

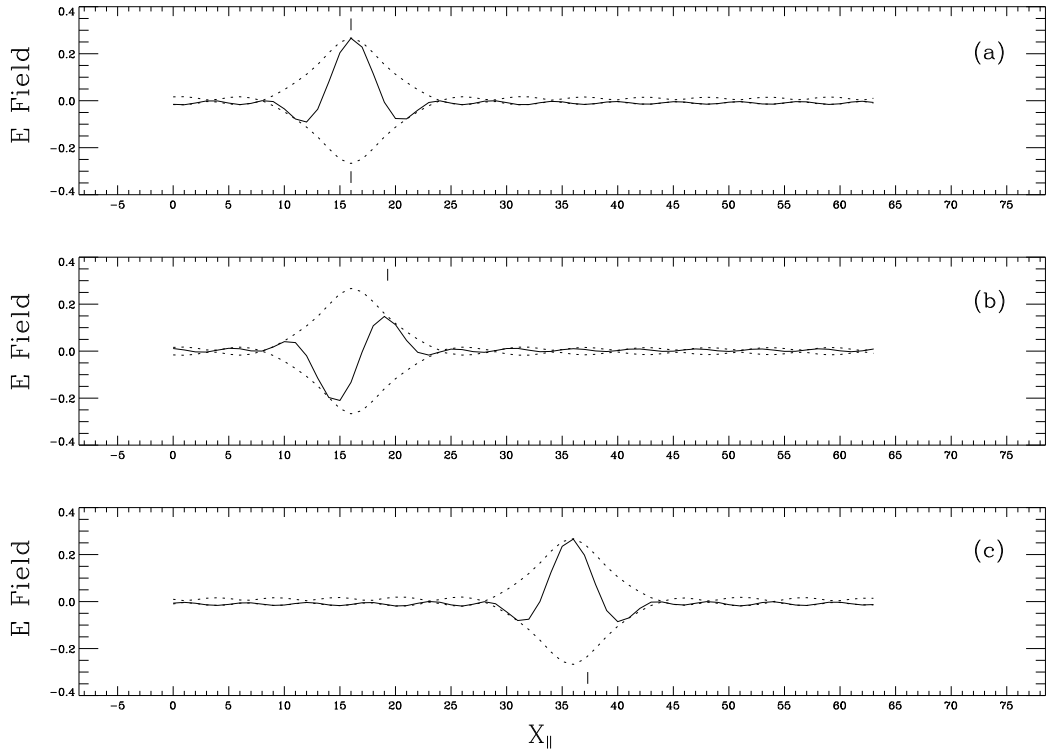

FIG. 8.—Solitary wavepacket at three times: (*a*) initial time; (*b*) after 20 time steps, $2\omega_p^{-1}$; and (*c*) after 3000 time steps, $300\omega_p^{-1}$. The solid line is the $E_\parallel$ field, and the dashed line is the field envelope in units $(8\pi nm\bar{v}_\parallel^2)^{1/2}$. The length scale is marked in grid units, c/ω_p. The upper/lower hatchmarks indicate theoretical positions of phase/envelope peaks.

TABLE 2

COMPARISON OF THEORETICAL AND NUMERICAL WAVE PARAMETERS

Description	Analytic Formula	Analytic Value	Simulation Value
Phase propagation distance at 20 time steps ($T = 2.0\omega_p^{-1}$)	$v_{ph}\,T$	$3.34c/\omega_p$	$3.0c/\omega_p$
Envelope propagation distance at 3000 time steps ($T = 300\omega_p^{-1}$)	$v_{gr}\,T$	$21.3c/\omega_p$	$20.0c/\omega_p$
HWHM at 3000 time steps ($T = 300\omega_p^{-1}$)	$L_{1/2}(1 + \beta^2T^2)^{1/2}$	$10.1c/\omega_p$	$9.0c/\omega_p$

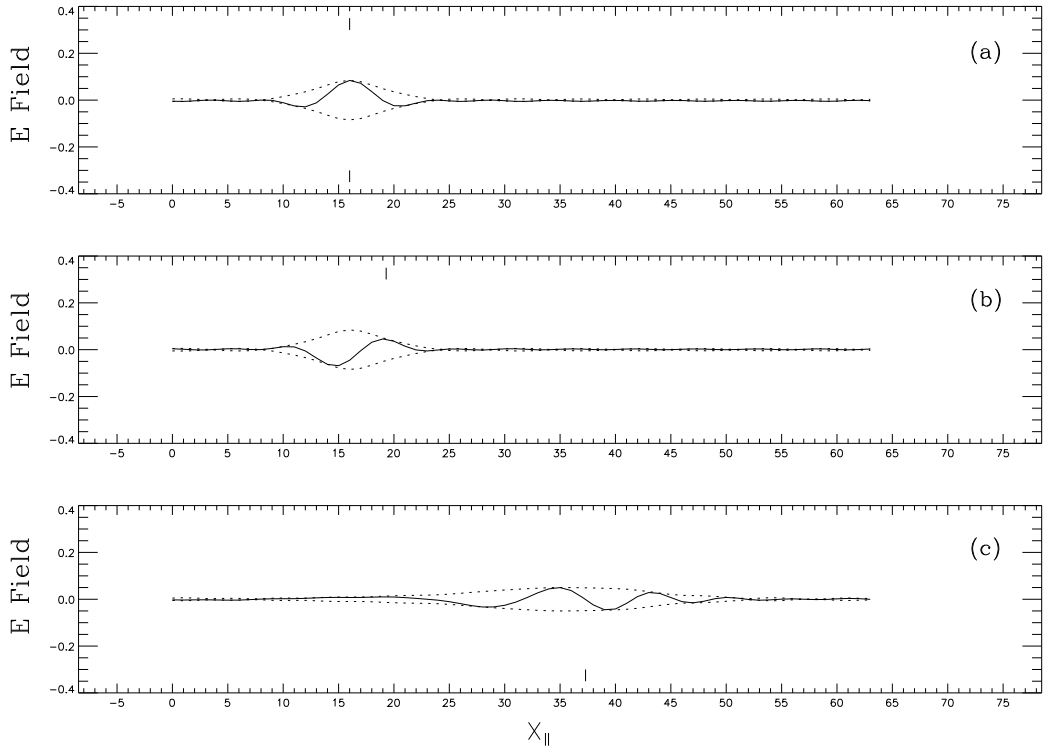

FIG. 9.—Linear wavepacket at the same times as in Fig. 8. Note dispersive broadening at later times.

REFERENCES

Arons, J. 1983, in AIP Conf. Proc. 101, Positron-Electron Pairs in Astrophysics, ed. M. Burns, A. K. Harding, & R. Ramaty (New York: AIP), 163
Arons, J., & Barnard, J. J. 1986, ApJ, 302, 120
Arons, J., & Scharlemann, E. T. 1979, ApJ, 231, 854
Asseo, E. 1993, MNRAS, 264, 940
Asseo, E., Pellat, R., & Rosado, M. 1980, ApJ, 239, 661
Asseo, E., Pelletier, G., & Sol, H. 1990, MNRAS, 247, 529
Buschauer, R., & Benford, G. 1977, MNRAS, 179, 99
Cheng, A. F., & Ruderman, M. A. 1977a, ApJ, 212, 800
———. 1977b, ApJ, 214, 598
Chian, A. C.-L. 1992, in IAU Colloq. 128, The Magnetospheric Structure and Emission Mechanisms of Radio Pulsars, ed. T. H. Hankins, J. M. Rankin, & J. A. Gil, (Zielona Gora: Pedagogical Univ. Press), 356
Daugherty, J. K., & Harding, A. K. 1983, ApJ, 273, 761
Goldman, M. V. 1984, Rev. Mod. Phys. 56, 709
Goldman, M. V., & Nicholson, D. R. 1978, Phys. Rev. Lett., 41, 406
Goldman, M. V., Weatherall, J. C., & Nicholson, D. R. 1981, Phys Fluids, 24, 668
Goldreich, P., & Julian, W. 1969, ApJ, 157, 869
Gurevich, A. V., & Pitaevskii, L. P. 1963, Soviet Phys.-JETP, 18, 855
Gurnett, D. A., Maggs, J. E., Gallagher, D. L., Kurth, W. S., & Scarf, F. L. 1981, J. Geophys. Res., 86, 8833
Hadžievski, Lj. R., Škorić, M. M., Rubenchik, A. M., Sharpiro, E. G., & Turitsin, S. K. 1990, Phys. Rev. A, 42, 3561
Hankins, T. H. 1971, ApJ, 169, 487
Hasegawa, A. 1970, Phys. Rev. A, 1, 1746
Heiles, C., & Rankin, J. M. 1971, Nature Phys. Sci., 97, 231
Hinata, S. 1976, Ap&SS, 44, 389
Jackson, J. D. 1975, Classical Electrodynamics (New York: Wiley), 303
Kato, K. G., Benford, G., & Tzach, D. 1983, Phys. Fluids, 26, 3636
Kennel, C. F., Fujimara, F. S., & Pellat, R. 1979, Space Sci. Rev., 24, 407
Krasnosel'skikh, V. V., & Sotnikov, V. I. 1977, Soviet J. Plasma Phys., 3, 491
Lin, R. P., Potter, D. W., Gurnett, D. A., & Scarf, F. L. 1981, ApJ, 251, 64
Melrose, D. B. 1992, in IAU Colloq. 128, The Magnetospheric Structure and Emission Mechanisms of Radio Pulsars, ed. T. H. Hankins, J. M. Rankin, & J. A. Gil, (Zielona Gora: Pedagogical Univ. Press), 307
Mikhailovskii, A. B., Onishchenko, O. G., & Tatarinov, E. G. 1985, Plasma Phys. Controlled Fusion, 27, 527
Mofiz, U. A., Bhuiyan, G. M., Ahmed, Z., & Asgar, M. A. 1988, Phys. Rev. A, 38, 5935
Mofiz, U. A., de Angelis, U., & Forlani, A. 1985, Phys. Rev. A, 31, 951
Newman, D. L., Goldman, M. V., & Ergun, R. E. 1994, Phys. Plasmas, 1, 1691
Nicholson, D. R., & Goldman, M. V. 1978, Phys. Fluids, 21, 1766
Nishikawa, K., & Liu, C. S. 1976, in Advances in Plasma Physics, Vol. 6, ed. A. Simon & W. B. Thompson (New York: Wiley), 3
Pelletier, G., Sol, H., & Asseo, E. 1988, Phys. Rev. A, 38, 2552
Robinson, P. A., Newman, D. L., & Goldman, M. V. 1988, Phys. Rev. Lett., 61, 702
Rowland, H. L. 1985, Phys. Fluids, 28, 190
Ruderman, M. A., & Sutherland, P. G. 1975, ApJ, 196, 51
Sanuki, H., & Schmidt, G. 1977, J. Phys. Soc. Japan, 42, 664
Schmidt, G. 1966, Physics of High Temperature Plasmas (New York: Academic)
Sturrock, P. A. 1971, ApJ, 164, 529
Vladimirov, S. V., Tsytovich, V. N., Popel, S. I., & Khakimov, F. Kh. 1995, Modulational Interactions in Plasmas (Boston: Kluwer)
Weatherall, J. 1994, ApJ, 428, 261
Weatherall, J. C., Nicholson, D. R., & Goldman, M. V. 1983, Phys. Fluids, 26, 1103
Zakharov, V. E. 1972, Soviet Phys.-JETP, 35, 908
———. 1975, Soviet Phys.-JETP Lett., 21, 221